- 1 Synthesis and Elucidation of Local Structure in Phase-Controlled Colloidal Tin Phosphide
- 2 Nanocrystals from Aminophosphines

- 4 Authors: Ingrid J. Paredes¹, Amani M. Ebrahim², Rito Yanagi^{1,3,4}, Anna M. Plonka², Shuzhen
- 5 Chen¹, Hanlu Xia¹, Scott Lee¹, Mersal Khwaja¹, Haripriya Kannan¹, Ajay Singh⁵, Sooyeon
- 6 Hwang⁶, Anatoly I. Frenkel^{2,7}, Ayaskanta Sahu¹

7

- 8 Affiliations:
- 9 ¹Department of Chemical and Biomolecular Engineering, New York University Tandon School of
- Engineering, 6 Metrotech Center, Brooklyn, New York, 11201, United States
- ²Department of Materials Science and Chemical Engineering, Stony Brook University, Stony
- 12 Brook, New York 11794, United States
- ³Department of Chemical and Environmental Engineering, Yale University, New Haven,
- 14 Connecticut, 06520, United States
- ⁴Energy Sciences Institute, Yale University, 810 West Campus Drive, West Haven, Connecticut,
- 16 06516, United States
- 17 ⁵Center for Integrated Nanotechnologies, Material Physics and Applications Division, Los Alamos
- National Laboratory, Los Alamos, New Mexico 87545, United States
- 19 ⁶Center for Functional Nanomaterials, Brookhaven National Laboratory, Upton, New York 11973,
- 20 United States
- ⁷Chemistry Division, Brookhaven National Laboratory, Upton, New York 11973, United States

22

*Correspondence to: asahu@nyu.edu, anatoly.frenkel@stonybrook.edu

Abstract The chemical versatility and rich phase behavior of tin phosphides has led to interest in their use for a wide range of applications including optoelectronics, thermoelectrics, and electrocatalysis. However, researchers have identified few viable routes to high-quality, phase-pure, and phase-controlled tin phosphides. An outstanding issue is the small library of phosphorus precursors available for synthesis of metal phosphides. We demonstrated that inexpensive, commercially available, and environmentally benign aminophosphines can generate various phases of colloidal tin phosphides. We manipulated solvent concentrations, precursor identities, and growth conditions to obtain Sn₃P₄, SnP, and Sn₄P₃ nanocrystals. We performed a combination of X-ray diffraction and transmission electron microscopy to determine the phase purity of our samples. X-ray absorption spectroscopy provided detailed analyses of the local structures of the tin phosphides. Keywords: metal phosphides, tin phosphide, colloidal synthesis, aminophosphines, nanocrystals

1. Introduction

1 2

Interest in nanoscale tin-based pnictides has recently grown, owing to the rich phase chemistry available from the multiple oxidation states demonstrated by tin (0, 2+, 4+).^{1, 2} Tin phosphides (SnP₃, Sn₃P₄, SnP, and Sn₄P₃) in particular have been investigated for thermoelectrics,³ photovoltaics,⁴ superconductance,⁵ catalysis,⁶⁻⁸ and as anodes for Na-ion and Li-ion batteries.⁹⁻³⁷ Still, synthesis of phase-pure tin phosphides remains as a barrier for widespread use in such applications. Tin phosphides exhibit various stoichiometries, and polymorphism has been observed for fixed stoichiometries, e.g. in SnP and Sn₃P₄.¹ Thus, developing facile and controlled syntheses of phase-pure tin phosphide nanostructures is essential to understanding and optimizing their use.

To date, few syntheses of nanoscale tin phosphides have been reported.^{17, 26, 33-35, 39-41} Researchers currently have a small library of expensive and dangerous phosphorus precursors available to them. Sn₃P₄, SnP, and Sn₄P₃ nanocrystals, for example, have been synthesized from the common phosphorus precursor tris(trimethylsilyl)phosphine.³⁹ Hexamethylphosphoramide has provided phase-pure SnP nanocrystals, but other phase-pure stoichiometries were inaccessible.⁴⁰ We present a new route to tin phosphide nanocrystals via tris(diethyl)aminophosphine. Aminophosphines are a class of inexpensive, environmentally benign phosphorus precursors that are safe to use in ambient conditions.⁴²⁻⁴⁸ Since their introduction, aminophosphines have been used to synthesize In, Co, Ni, Fe and Cd, and Cu- phosphides.⁴³⁻⁴⁷ Unlike tris(trimethylsilyl)phosphine, a P(-III) source ready for reaction, aminophosphines first undergo a series of redox reactions to form an active phosphorus precursor. In previous work, combining aminophosphines with different metal

- 1 halide precursors altered reaction kinetics. We explored using a similar approach to synthesize
- 2 Sn₄P₃, SnP, and Sn₃P₄ nanocrystals.

- 4 We present structural and chemical characterization of our materials using X-ray diffraction
- 5 (XRD), transmission electron microscopy (TEM), X-ray photoelectron spectroscopy (XPS) and
- 6 X-ray absorption spectroscopy (XAS). XRD and TEM are conventional techniques that provided
- 7 the morphology and crystal structures of our samples. XPS and XAS allowed us to investigate
- 8 oxidation states and corresponding local environments of tin in tin phosphides. Characterization
- 9 of the oxidation states of various tin phosphides remain a current topic of interest. Results have
- been mixed, with multiple oxidation states observed in both SnP and Sn₄P₃. Even less is known
- about Sn₃P₄. Our characterization methodology aims to provide insight on the coordination
- 12 environments of tin in nanostructured tin phosphides.

2. Materials and Methods

13 14 15

2.1 Materials

- Ethanol (anhydrous, 200 proof, \geq 99.5%), oleic acid (technical grade, 90%), oleylamine (technical
- grade, 70%), tin (II) bromide (anhydrous, 99.999% trace metal basis), tin (II) iodide (anhydrous,
- powder, 99.999%, trace metals basis), toluene (anhydrous, 99.8%), trioctylamine (98%),
- tris(diethylamino)phosphine (97%), trioctylphosphine (97%), zinc (II) bromide (anhydrous,
- 20 99.999% trace metal basis), zinc (II) chloride (anhydrous, 99.999% trace metal basis), and zinc
- 21 (II) iodide (anhydrous, 99.999% trace metal basis), were purchased from Sigma Aldrich. Tin (II)
- 22 chloride (anhydrous, 98%) was purchased from Alfa Aesar. All chemicals were used without
- 23 further purification after their purchase. Anhydrous chemicals were purchased and stored in the
- 24 glovebox. Extra care was used when handling tin halides and zinc halides, which are hygroscopic.

2 Please note that quenching of the following reactions requires injection of toluene at 90 °C. We

encourage caution when replicating our work, as injection of toluene above its boiling point

(110 °C) can cause harm.

5

6

9

10

11

12

13

3

4

2.2 Synthesis of Trigonal Sn₃P₄ Nanocrystals

7 Tin (II) chloride (SnCl₂) (256.0 mg, 1.35 mmol), zinc (II) chloride (ZnCl₂) (184.0 mg,1.35 mmol),

8 oleylamine (20 mL), and oleic acid (1 mL) were mixed in a 100 mL three-neck flask. The reaction

mixture was degassed under vacuum at 120 °C, producing a clear, yellow solution that was then

heated under nitrogen to 250 °C. At 250 °C, P(NEt₂)₃ (1.6 mL, 4 mmol) was rapidly injected into

the flask, producing a black dispersion that was left for 2 min. After 2 min, the reaction was cooled

slowly to room temperature. The reaction mixture was then transferred to a nitrogen-filled

glovebox for extraction and cleaning.

14

15

16

17

18

19

In a typical purification process, Sn₃P₄ nanocrystals were precipitated from ethanol via

centrifugation at 6000 rpm for 5 min. The precipitated nanocrystals, a black powder, were then

washed with toluene (5 mL) by centrifugation at 2000 rpm for 5 min to precipitate out extra

surfactants and unreacted precursors. The supernatant was extracted, the dispersed particles were

crashed out with ethanol, and finally the nanoparticles were dried under vacuum and stored as a

dry powder in the glovebox.

21

2.3 Synthesis of Trigonal SnP Nanocrystals

- 2 SnCl₂ (256.0 mg, 1.35 mmol), ZnCl₂ (184.0 mg, 1.35 mmol), oleylamine (40 mL) and oleic acid
- 3 (1 mL) were mixed in a 100 mL three-neck flask. The reaction mixture was degassed under
- 4 vacuum at 120 °C, producing a clear, yellow solution that was then heated under nitrogen to
- 5 250 °C. At 250 °C, P(NEt₂)₃ (1.6 mL, 4 mmol) was rapidly injected into the flask, producing a
- 6 black dispersion that was left for 2 min. The reaction was then quenched in three steps. First, a
- 7 heat gun on the "cool" air setting was used until the reaction temperature fell to 200 °C. Then, a
- 8 room temperature water bath was introduced to further cool the reaction. Finally, toluene (20 mL)
- 9 was injected at 90 °C to complete the quenching procedure.

10

1

- 11 The reaction mixture was transferred to a nitrogen-filled glovebox for purification and extraction.
- 12 In a typical purification process, SnP nanocrystals were precipitated from ethanol via
- centrifugation at 6000 rpm for 5 min. The precipitated nanocrystals, a black powder, were then
- washed with toluene (5 mL) by centrifugation at 2000 rpm for 5 min to precipitate out extra
- surfactants and unreacted precursors. The supernatant was extracted, the dispersed particles were
- crashed out with ethanol, and finally the nanoparticles were dried under vacuum and stored as a
- 17 dry powder in the glovebox.

18

19

2.4 Synthesis of Rhombohedral Sn₄P₃ Nanocrystals

- 20 SnCl₂ (256.0 mg, 1.35 mmol), ZnCl₂ (184.0 mg, 1.35 mmol), oleylamine (15 mL), trioctylamine
- 21 (5 mL), and oleic acid (1 mL) were mixed in a 100 mL three-neck flask. The reaction mixture was
- degassed under vacuum at 120 °C, producing a clear, yellow solution that was then heated under
- 23 nitrogen to 250 °C. At 250 °C, P(NEt₂)₃ (1.6 mL, 4 mmol) was rapidly injected into the flask,

- 1 producing a black dispersion that was left for 2 min. The reaction was then quenched in three steps.
- 2 First, a heat gun on the "cool" air setting was used until the reaction temperature fell to 200 °C.
- 3 Then, a room temperature water bath was introduced to further cool the reaction. Finally, toluene
- 4 (20 mL) was injected at 90 °C to complete the quenching procedure.

- 6 The reaction mixture was transferred to a nitrogen-filled glovebox for purification and extraction.
- 7 In a typical purification process, Sn₄P₃ nanocrystals were precipitated from ethanol via
- 8 centrifugation at 6000 rpm for 5 min. The precipitated nanocrystals, a black powder, were then
- 9 washed with chloroform (5 mL) by centrifugation at 2000 rpm for 5 min to precipitate out extra
- surfactants and unreacted precursors. The supernatant was extracted, and the dispersed particles
- were crashed out with ethanol. Finally, the nanoparticles were dried under vacuum and stored as a
- 12 dry powder in the glovebox.

13

14

2.5 Characterization

- 15 TEM and XRD measurements were used to study the morphology and phase of the synthesized
- 16 nanocrystals. Energy dispersive X-ray spectroscopy (EDX) determined relative stoichiometry.
- 17 XPS and XAS measurements provided the chemical composition and local environment of our
- materials. Details of sample preparation, experimental conditions, and analysis procedures can be
- 19 found in the Supporting Information (**ESI**).

20

3. Results and Discussion

21 22

23 3.1 Synthesis of Tin Phosphide Nanocrystals

Sn₃P₄, SnP, or Sn₄P₃ nanocrystals were synthesized via hot injection of P(NEt₂)₃ into a mixture of amine solvents, oleic acid, zinc halides, and tin halides (**Table S1**). We introduced zinc halides into the reaction mixture following the example of InP syntheses, where zinc halide choice influenced particle size.⁴⁵ Zinc halides have been found to promote the formation and stabilization

of activated precursors for growth via Zn-N-P intermediates.⁴⁹ We thus began our work by

investigating the role of zinc in aminophosphine-based routes to tin phosphides.

present, Sn₄P₃ impurities in SnP have been previously reported.³⁹

We began our study with ZnCl₂ and SnCl₂, as dichlorides have been most used in previous aminophosphine-based routes to metal phosphides.⁴²⁻⁴⁸ XRD data were indexed to trigonal SnP with rhombhedral Sn₄P₃ as an impurity phase (**Figure 1a**). We note that in the bulk, SnP is a metastable phase formed only at high temperature and high pressure, while Sn₄P₃ is the thermally stable phase of tin phosphide.⁵⁰ Nanocrystals often stabilize in metastable phases because of their large surface energies.⁵¹ While our data were insufficient to estimate the amount of each phase

Bright field TEM images showed that the average diameter of the nanoparticles was 25 ± 3.9 nm (**Figure 1b**). Under closer inspection in HRTEM, we observed a d-spacing of 3.27 Å, indexed to the characteristic <101> peak of trigonal SnP (**Figure 1c**). Assignment of SnP to the structure was consistent with EDX measurements, which approximated an Sn:P ratio of 1:1 (**Figure 1d**). In HRTEM and EDX, we also observed an amorphous layer of oxidized tin at the surface of the nanocrystals (**Figure 1c**, **d**). We note that no XRD peaks were indexed to tin oxides or tin phosphates in samples that were freshly prepared for use in diffraction studies. Still, metal phosphides readily oxidize. While exposure to air was minimized, sample oxidation may have

- 1 occurred during transportation to the microscopy facility (from Brooklyn, NY to Berkeley, CA) or
- 2 during sample loading.

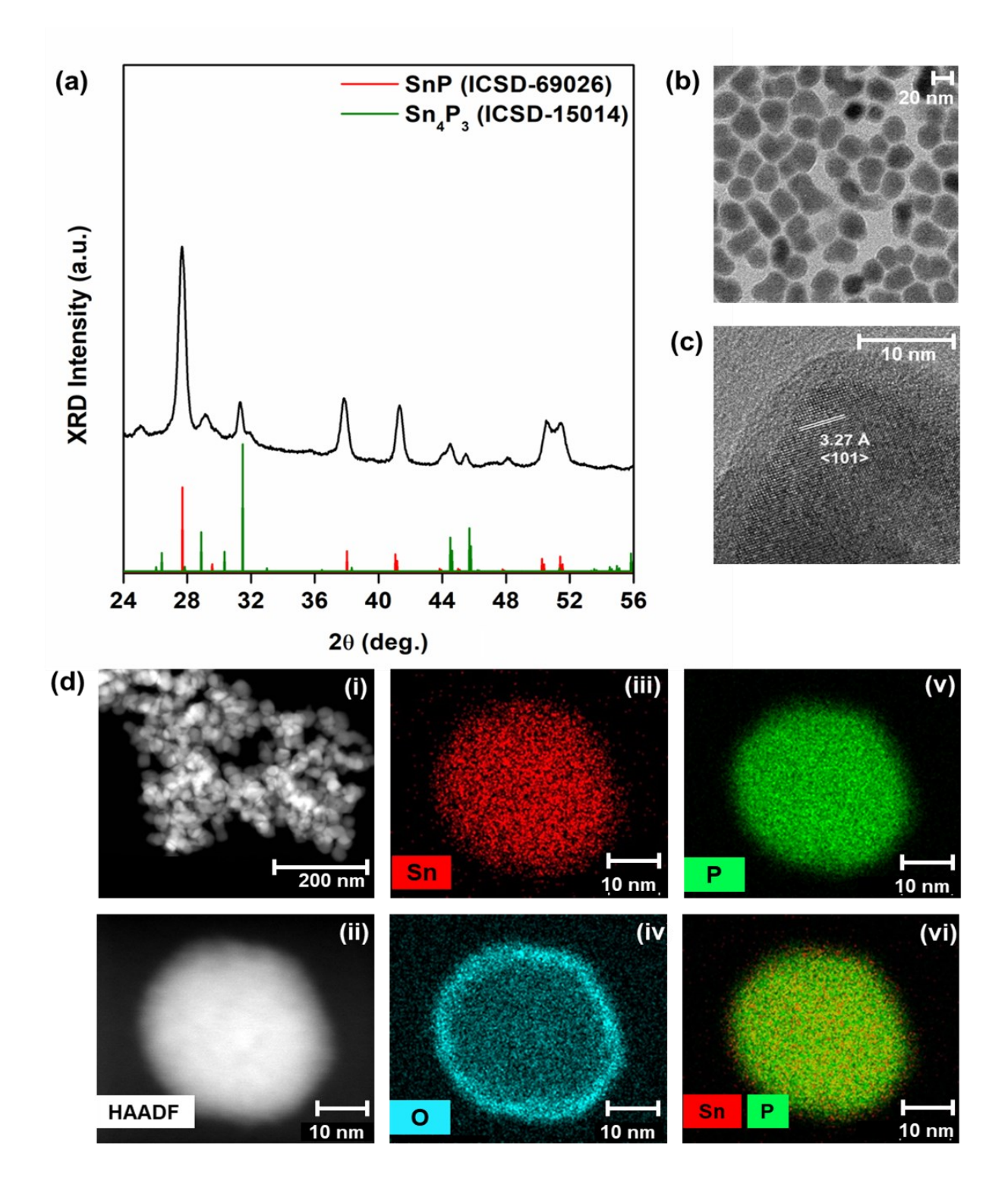


Figure 1. Phase and morphology of tin phosphide nanocrystals. The nanoparticles were grown for 2 min following the injection of tris(diethyl)aminophosphine ((PNEt₂)₃) at 250 °C. (a) X-ray diffraction (XRD) data for synthesized nanocrystals (black) were indexed to SnP (red, ICSD-69026), with trace amounts of Sn_4P_3 present (green, ICSD-15014). (b) Bright field transmission electron microscopy (TEM) images of synthesized nanocrystals revealed that they were 25 ± 3.9

nm in diameter. (c) High resolution transmission electron microscopy (HRTEM) showed d-

2 spacings of 3.27 Å, corresponding to the characteristic <101> peak of SnP. We observed oxidation

at the surface of the nanocrystals due to exposure to air prior to the HRTEM measurement. (d)

4 Scanning transmission electron microscopy (STEM) and high-angle annular dark field (HAADF)

5 images for nanocrystals show elemental mapping for Sn, O, and P. The overlay of Sn and P maps

6 provided an approximate Sn:P ratio of 1:1.

7 Phase mixtures were previously observed in cobalt phosphides obtained from aminophosphines

8 and cobalt dihalides. 46 Thus, to further investigate these results, we synthesized tin phosphides

from several combinations of tin and zinc dihalides (**Table 1**). Experiments using SnCl₂ and SnBr₂

provided phase mixtures of SnP, Sn₄P₃, and Sn₃P₄ (Figure 2a, b). Using SnI₂, we obtained phase-

pure SnP (Figure 2c).

Table 1. Phases of Tin Phosphides Obtained with Different Tin and Zinc Halides

	Zinc Halide		
Tin Halide	$ZnCl_2$	ZnBr ₂	ZnI_2
SnCl ₂	$SnP + Sn_4P_3$	$SnP + Sn_4P_3$	$Sn_4P_3 + SnP$
SnBr_2	$SnP + Sn_4P_3$	$SnP + Sn_4P_3 + Sn_3P_4$	No products obtained
SnI_2	SnP	SnP	No products obtained

13

14

15

16

17

18

19

20

9

10

11

12

We attributed our results to the relative dissociation energies of the halides (M-I < M-Br < M-Cl).

Based on the dissociation energies of the halides, Sn—P monomers would form most easily from

iodides, followed by bromides, then chlorides. Our results obtained from reactions combining SnI_2

with ZnCl₂ or ZnBr₂ supported this reasoning. The reaction occurred as expected, reducing SnI₂

to produce phase-pure SnP. However, combining SnI₂ with ZnI₂ was unsuccessful. In this instance,

we noticed a dangerous over pressurization of the reaction flask upon injection of P(NEt₂)₃.

Attempts to reduce the pressure did not improve the result, and so these experiments were forgone.

- 1 The over pressurization may have occurred due to the formation of diethylamine made possible by
- 2 the ready dissociation of M—I complexes.

- 4 Still, the results obtained from SnCl₂ and SnBr₂ were more complicated. We obtained phase
- 5 mixtures of tin phosphides, with the dominant phase changing depending on the halide used. We
- 6 note that the role of zinc in these reactions is still under investigation. In all experiments, the ratio
- 7 of zinc to tin halide was held constant at 1:1. Maintaining this ratio of Zn:Sn was essential to obtain
- 8 identifiable products. When we altered the relative stoichiometry of zinc to tin or removed zinc
- 9 from the reaction, we could not obtain any phase-pure materials (Figure S1). As mentioned
- 10 previously, zinc halides form Zn-N-P intermediates that promote the formation activated
- precursors for growth. These intermediates can undergo competing processes that can modify
- 12 reaction equilibria.⁴⁹

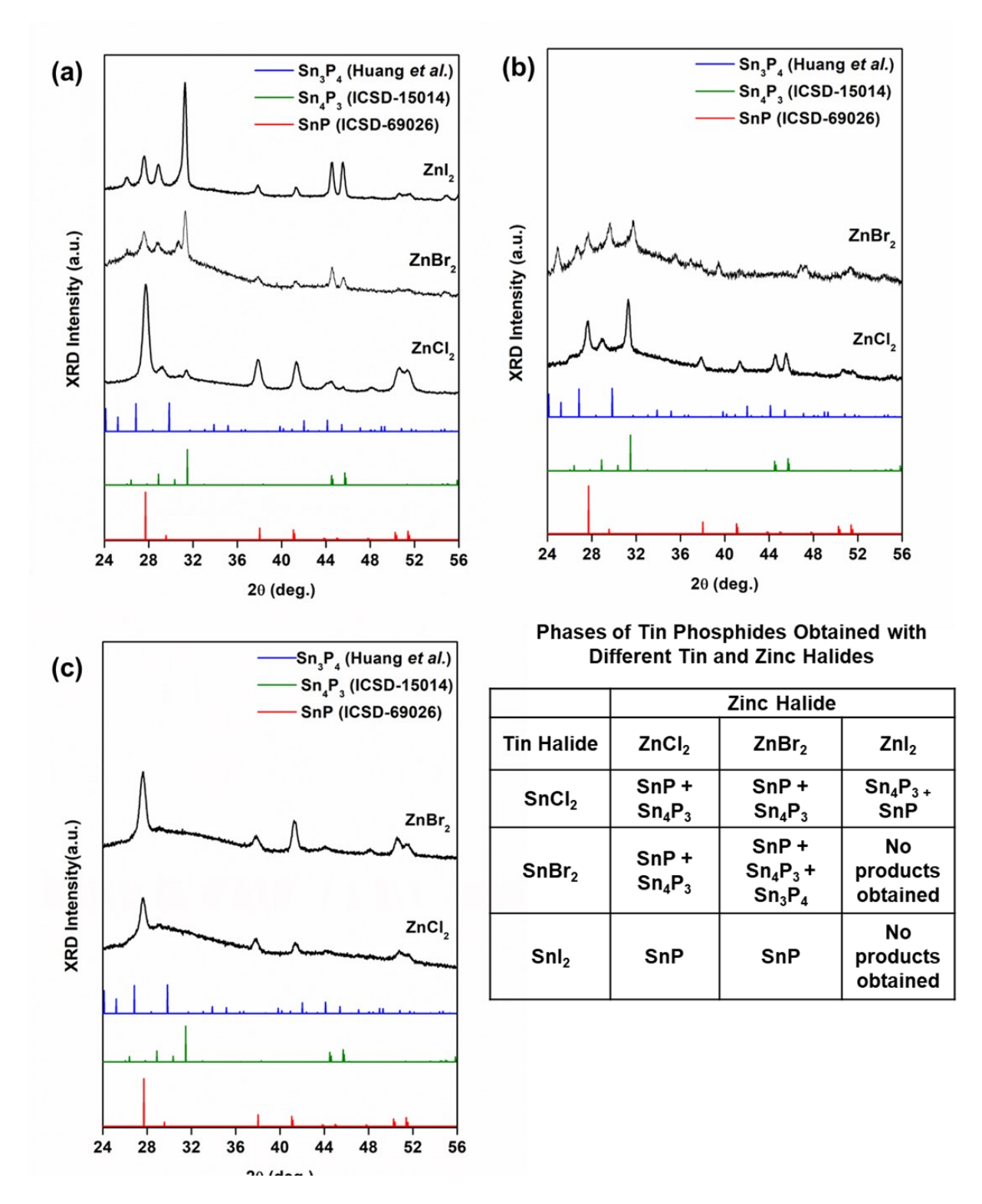


Figure 2. X-ray diffraction (XRD) data obtained for tin phosphide nanocrystals grown with various combinations of and SnX_2 and ZnX_2 (X = Cl⁻, Br⁻, and l⁻) precursors. Nanocrystals were grown for 2 min following injection of tris(diethyl)aminophosphine (P(NEt₂)₃) at 250 °C. Data is plotted against reference data for SnP (red, ICSD-69026), Sn_4P_3 (green, ICSD-15014) and Sn_3P_4 (blue, Huang *et al.*). In each experiment, a 1:1 ratio of Zn:Sn was used. (a) Holding SnCl₂ constant,

- phase mixtures of SnP and Sn₄P₃ using ZnX₂. (b) Similarly, holding SnBr₂ constant, phase
- 2 mixtures of SnP, Sn₄P₃, and Sn₃P₄ were obtained from experiments with ZnCl₂ and ZnBr₂.
- 3 Experiments with ZnI₂ were unsuccessful. (c) Holding SnI₂ constant, phase-pure SnP nanocrystals
- 4 were obtained with ZnCl₂ and ZnBr₂. Experiments with ZnI₂ were unsuccessful.
- 5 Previous work has shown that reaction kinetics vary with the ratio of P(NEt₂)₃ to primary amine
- 6 solvent. This is because the amine plays two roles in the reaction; the solvent activates P(NEt₂)₃
- 7 and complexes the metal halide. In its first role, activation occurs via transamination (Scheme 1).

Scheme 1. Transamination of tris(aminophosphines) with primary amines

$$P(NEt_2)_3 + RNH_2 \leftrightarrow P(NEt_2)_2 (NHR) + Et_2NH$$
 (1)

$$P(NEt_2)_2(NHR) + RNH_2 \leftrightarrow P(NEt_2)(NHR)_2 + Et_2NH$$
 (2)

$$P(NEt_2)_2(NHR)_2 + RNH_2 \leftrightarrow P(NHR)_3 + Et_2NH$$
(3)

- 8 The reaction is driven by the evaporation of diethylamine (Et₂NH, with a boiling point of 7 °C) at
- 9 reaction temperature. As the dialkylamine evaporates, the equilibrium shifts the reaction towards
- production of the final transamination product, P(NHR)₃. Buffard *et al.* found that ratio of P(NEt₂)₃
- 11 to oleylamine changed the transamination products present.⁴⁴ They identified a minimum amount
- of oleylamine required to produce quality nanocrystals, as we have observed in our work (**Table**
- 13 **2**).
- We thus investigated the kinetics of this reaction first by tuning solvent volume (**Table 2**). We
- 15 hypothesized that changing the ratio of oleylamine to P(NEt₂)₃ would drive the reaction towards
- phase-pure SnP or Sn_4P_3 . With more oleylamine present to activate $P(NEt_2)_3$, we expected to form
- of phase-pure SnP; with less, we expected to form of Sn-rich Sn₄P₃. In our work, doubling the
- amount of oleylamine from a 15:1 ratio of oleylamine to P(NEt₂)₃ to a 30:1 ratio provided phase-
- pure, trigonal SnP nanocrystals (Figure 3a). The particles were 40 ± 7.0 nm in size, with the
- observed d-spacing consistent with that of the <101> peak of SnP (Figures 3b, c). STEM-EDX

- 1 measurements confirmed a stoichiometry of 1:1 Sn:P (Figure 3d). Halving the ratio, however,
- 2 provided a complicated phase mixture inseparable from remaining reactants in the solution
- 3 (Figure S2). The role of Zn-N-P intermediates in our reaction may have become more influential
- 4 at this scale, changing disproportionation reactions. Buffard et al. and Mundy et al. saw similar in
- 5 their work with other phosphide systems. 44, 46
- 6 To confirm the validity of this trend, we performed a control experiment where transamination and
- 7 nucleation were separated. The "two-pot" protocol was adapted from work by Rachkov et al. 47
- 8 Oleylamine and P(NEt₂)₃ were reacted under vacuum for 3 hours, and the resulting transamination
- 9 product was then injected into the mixture of zinc and tin halides, oleylamine, and oleic acid at
- 10 250 °C. In the two-pot case, the results followed the trend observed in the one-pot experiment;
- increasing the amount of oleylamine present drove the reaction pathway towards SnP, and away
- from a phase mixture of SnP and Sn₄P₃ (**Figure S3**).

Table 2. Phases of Tin Phosphides Obtained with Varying Amounts of Oleylamine

Volume (ml)	Oleylamine:P(NEt ₂) ₃	Phase
10	7.5:1	Unidentified phase mixture
20	15:1	$SnP + Sn_4P_3$
40	30:1	SnP

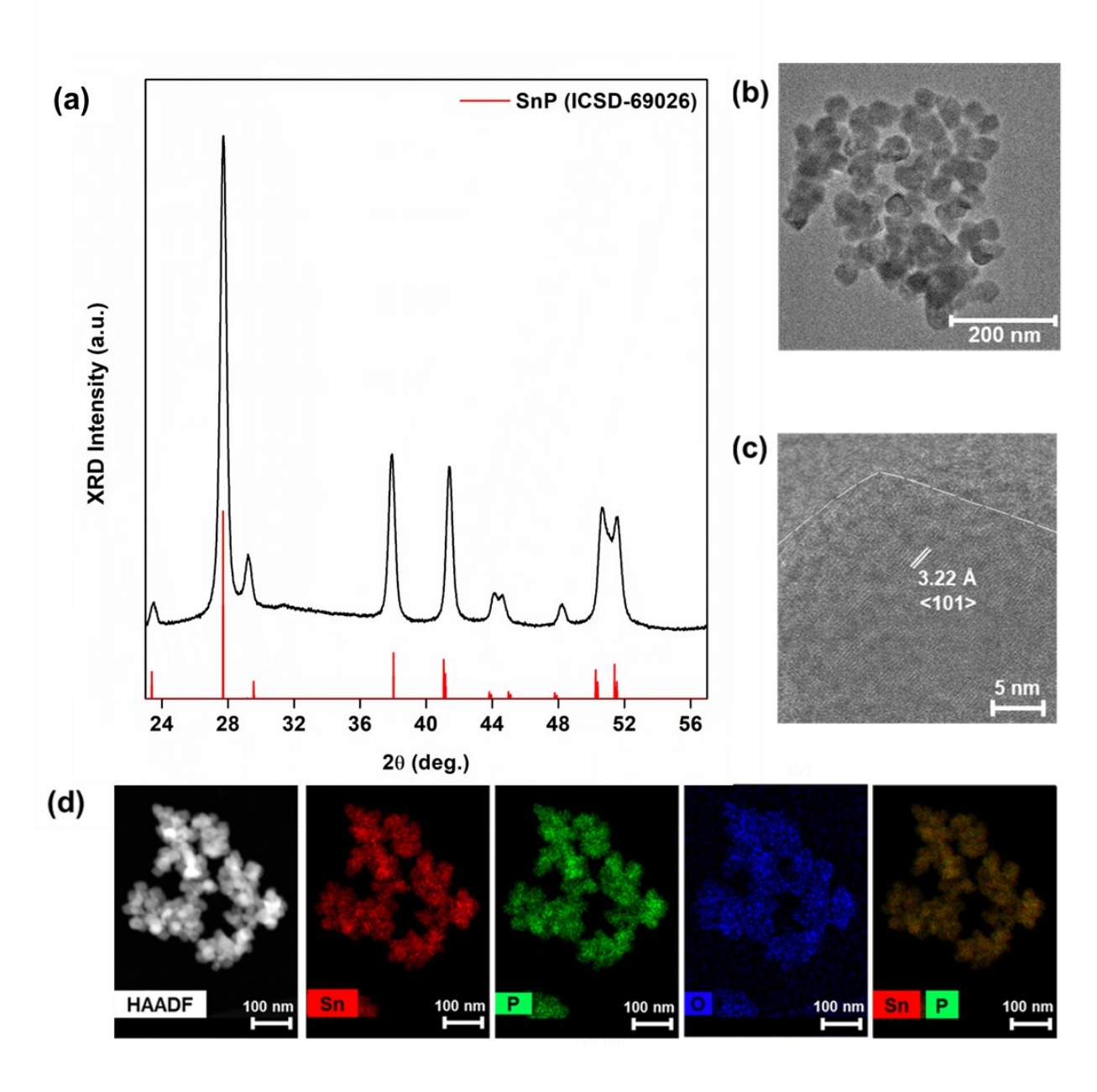


Figure 3. Phase and morphology data for phase-pure SnP nanocrystals grown for 2 min at 250 °C following injection of tris(diethyl)aminophosphine (PNEt₂)₃ into 40 mL of oleylamine and equimolar amounts of SnCl₂ and ZnCl₂. (a) X-ray diffraction data (XRD) obtained for synthesized trigonal SnP nanocrystals plotted against reference data for trigonal SnP (ICSD-69026). (b) Bright field transmission electron microscopy (TEM) revealed that the SnP nanocrystals were 40 ± 7.0 nm in diameter. (c) High resolution TEM (HRTEM) images showed crystalline particles with an amorphous layer on its surface. (d) Scanning transmission electron microscopy High-angle annular dark-field (STEM-HAADF) image and corresponding elemental mapping for Sn, O, and P. The overlay approximated an Sn:P ratio of 1:1.

- 1 The SnP tin phosphide nanocrystals exhibited poor stability (**Figure 3b**). While the particles were
- 2 visibly colloidally stable, aggregation still occurred (Figure S4). We attempted to stabilize the
- 3 particles using the co-solvents trioctylphosphine (TOP) and trioctylamine (Table 3).
- 4 Trioctylamine was previously used to stabilize InP nanocrystals synthesized from
- 5 aminophosphines. 44 TOP was previously used to stabilize tin phosphide nanocrystals. 39

Table 3. Phases of Tin Phosphides Obtained with Addition of Cosolvents

Cosolvent	Volume (mL)	Phase	
Trioctylamine	5	Sn ₄ P ₃	
	10	$SnP + Sn_4P_3 + Sn_3P_4$	
	15	$SnP + Sn_4P_3 + Sn_3P_4$	
Trioctylphosphine	0.15	$Sn_3P_4 + SnP$	
	0.6	$Sn_3P_4 + SnP$	
	3	$Sn_3P_4 + SnP$	

We found that a mixture of trioctylamine to oleylamine shifted the reaction pathway away from SnP to other tin phosphide phases. With 25 vol% of oleylamine replaced with trioctylamine, the effective ratio of amine to $P(NEt_2)_3$ was reduced, producing less $P(NHR)_3$ and shifting the direction of the reaction towards Sn-rich Sn₄P₃ (**Figure 4**). An unidentified minor impurity phase was also observed. Scherrer analysis approximated that the Sn₄P₃ nanoparticles were approximately 20.2 nm in diameter (**ESI, Section 1.1.2**); size could not be confirmed via TEM as the particles could not be completely isolated. With increased amounts of trioctylamine, we obtained phase mixtures of Sn₃P₄, SnP, and Sn₄P₃ (**Figure S5**). We attributed the change in reaction pathway to shifts in the equilibrium of transamination depending on the concentration of the amine consumed. If only oleylamine participates in transamination, the reaction occurs between $P(NEt_2)_3$ and $P(NHR)_3$ (R = methyl or ethyl group), which forms a dative bond with SnX₂.

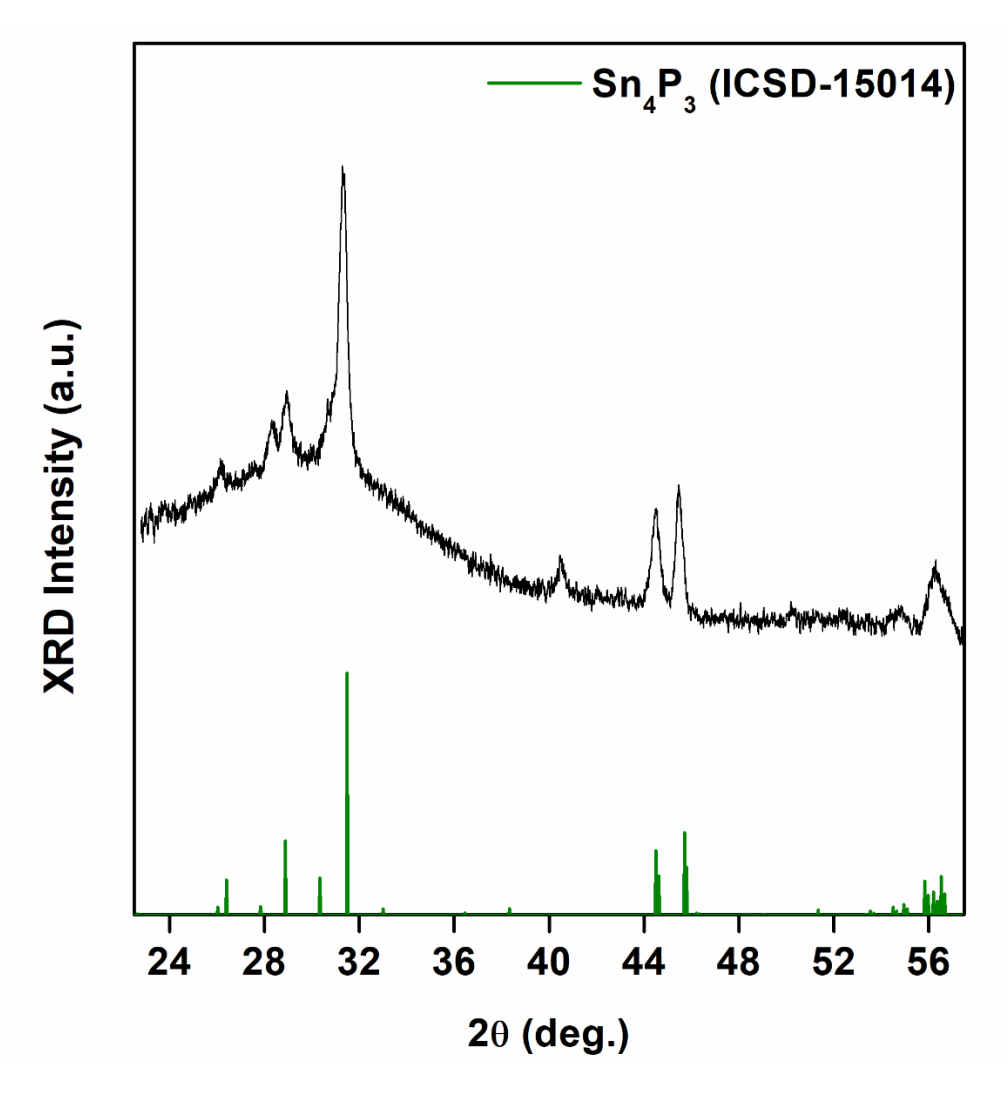


Figure 4. X-ray diffraction data obtained for synthesized Sn_4P_3 nanocrystals plotted against reference data for rhombohedral Sn_4P_3 (ICSD-15014). Nanocrystals were grown for 2 min at 250 °C following injection of tris(diethyl)aminophosphine (P(NEt₂)₃) into a 25/75 (v/v) mixture of trioctylamine to oleylamine.

When we performed reactions with TOP, we obtained Sn₃P₄ nanocrystals with an SnP impurity phase (**Figure 5**). We obtained this mixture across the range of temperatures of experiments performed (**Figures S6**). The successful synthesis of bulk Sn₃P₄ has required a high vapor pressure of phosphorus to provide phase-pure crystals.⁵² We suspect that the presence of phosphorus byproducts formed during transamination may have analogously elevated the phosphorus activity. Furthermore, colloidal synthesis provides routes to phases unattainable in the bulk.⁵³ The XRD

- pattern was comparable to a structure predicted by Huang et al. Nanocrystals were 8.3 ± 2.8 nm
- 2 in diameter. EDX measurements demonstrated an Sn:P ratio of 0.8 ± 0.2 , approximately Sn_3P_4
- 3 (Figure S7). To the best of our knowledge, this is the first report of crystalline Sn₃P₄ nanoparticles.

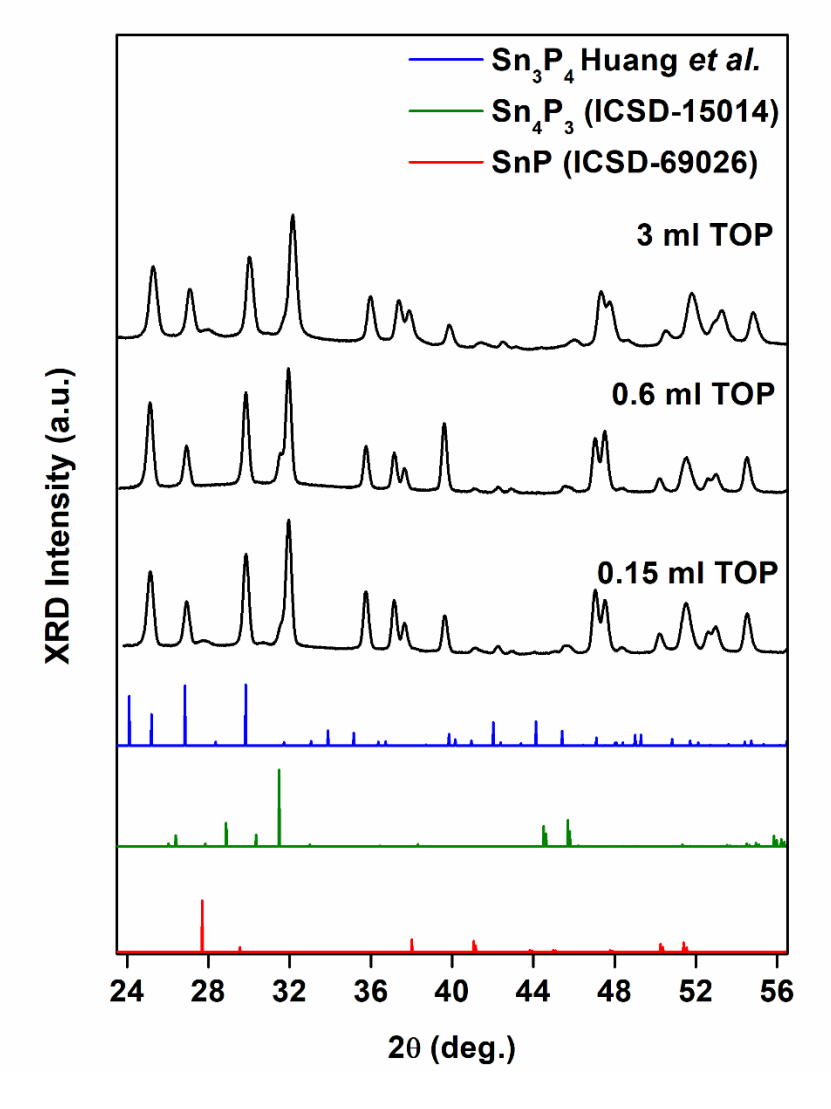


Figure 5. X-ray diffraction (XRD) data for Sn_3P_4 nanocrystals grown for 2 min at 250 °C following injection of tris(diethyl)aminophosphine ((PNEt₂)₃) in the presence of 0.15 mL, 0.6 mL, and 3 mL TOP. The data was compared to trigonal SnP (ICSD-69026), rhombohedral Sn_4P_3 (ICSD-15014), and trigonal Sn_3P_4 (Huang *et al.*⁵⁶)

3.2 Chemical Characterization of Tin Phosphide Nanocrystals

1 Understanding the local environment of tin is necessary to understand its use in various

2 applications. The presence of several tin oxidation states (Sn⁰, Sn²⁺, and Sn⁴⁺) within the same

crystal structure has hindered studies to date. We use XPS and XAS to provide insight into the

chemical environment of tin in SnP, Sn₃P₄, and Sn₄P₃.

5

8

9

10

11

12

13

14

15

16

17

18

3

4

Through XPS, we measured binding energies of Sn(3d_{3/2}) and P(2p_{3/2}) in our nanocrystals (**Figure 6. Figure S8-S10**). The experimental Sn(3d_{5/2}) binding energies were consistent with reported

6, Figure S8-S10). The experimental Sn(3d_{5/2}) binding energies were consistent with reported

results for tin phosphide nanocrystals. 34 For Sn_3P_4 , we observed two peaks, at 484.6 eV and 486.2

eV. We attributed the peak at 484.6 eV to metallic Sn and the peak at 486.2 eV to Sn²⁺.39,54 For

SnP, we observed a peak at 485 eV, suggesting metallic Sn bonding as previously described.⁵⁵ For

Sn₄P₃, we observed a broad peak at 486.2 eV, suggesting the presence of multiple oxidation states.

To date, formal charges for Sn in rhombohedral Sn₄P₃ have not been assigned. Evidence of metallic

bonding like that of β -Sn has been observed, while XAS data have suggested Sn-P and Sn-P-Sn

bonding structure. 10, 56, 57 Mixed oxidation states may have also been present due to surface

oxidation, as observed in TEM. Evidence of oxidation was also observed in experimental P(2p_{3/2})

binding energies, which showed a peak at 133 eV, typical of metal phosphates. Binding energies

below 130 eV, characteristic to metal phosphides, were dominant; the binding energy slightly

decreased with increasing phosphorus content. While this trend has been observed in other metal

phosphides, the exact nature of these shifts has not been determined.⁵⁸

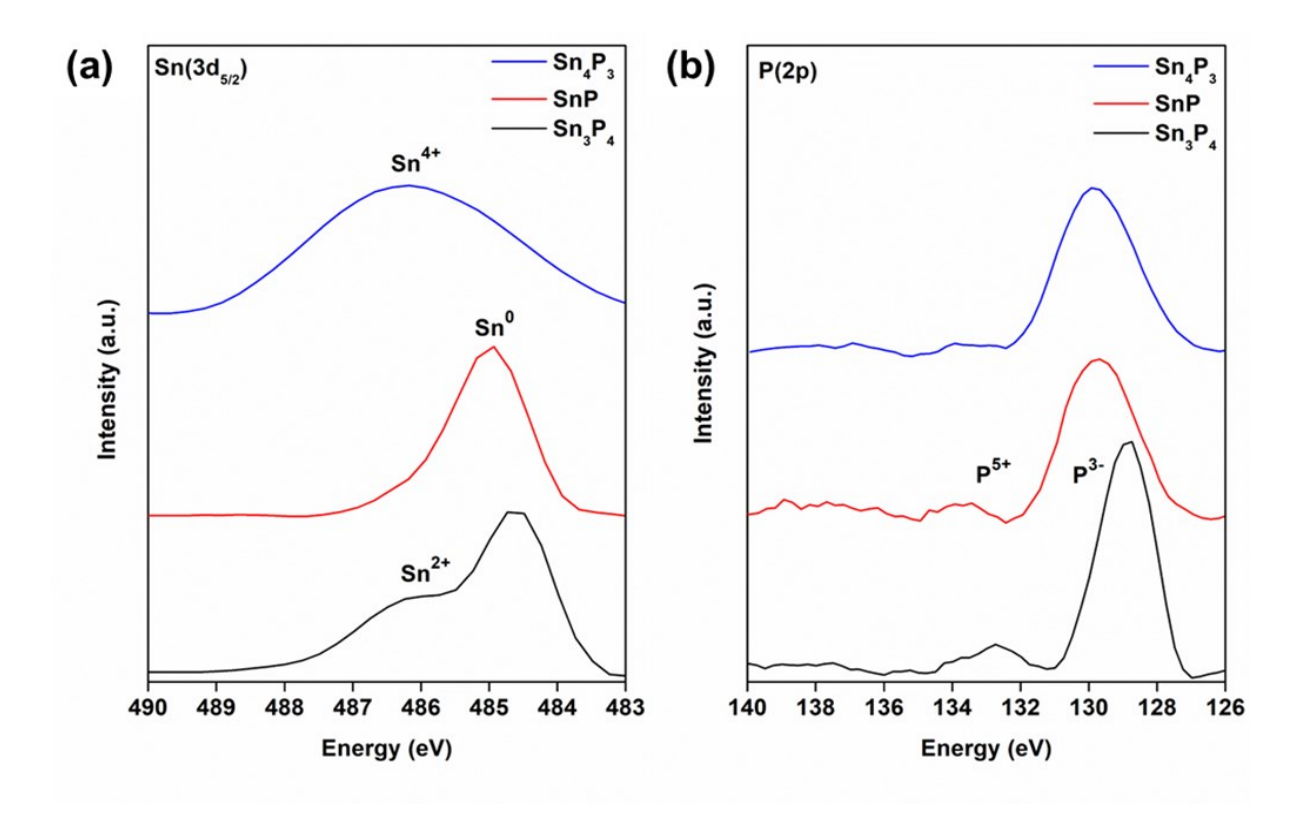
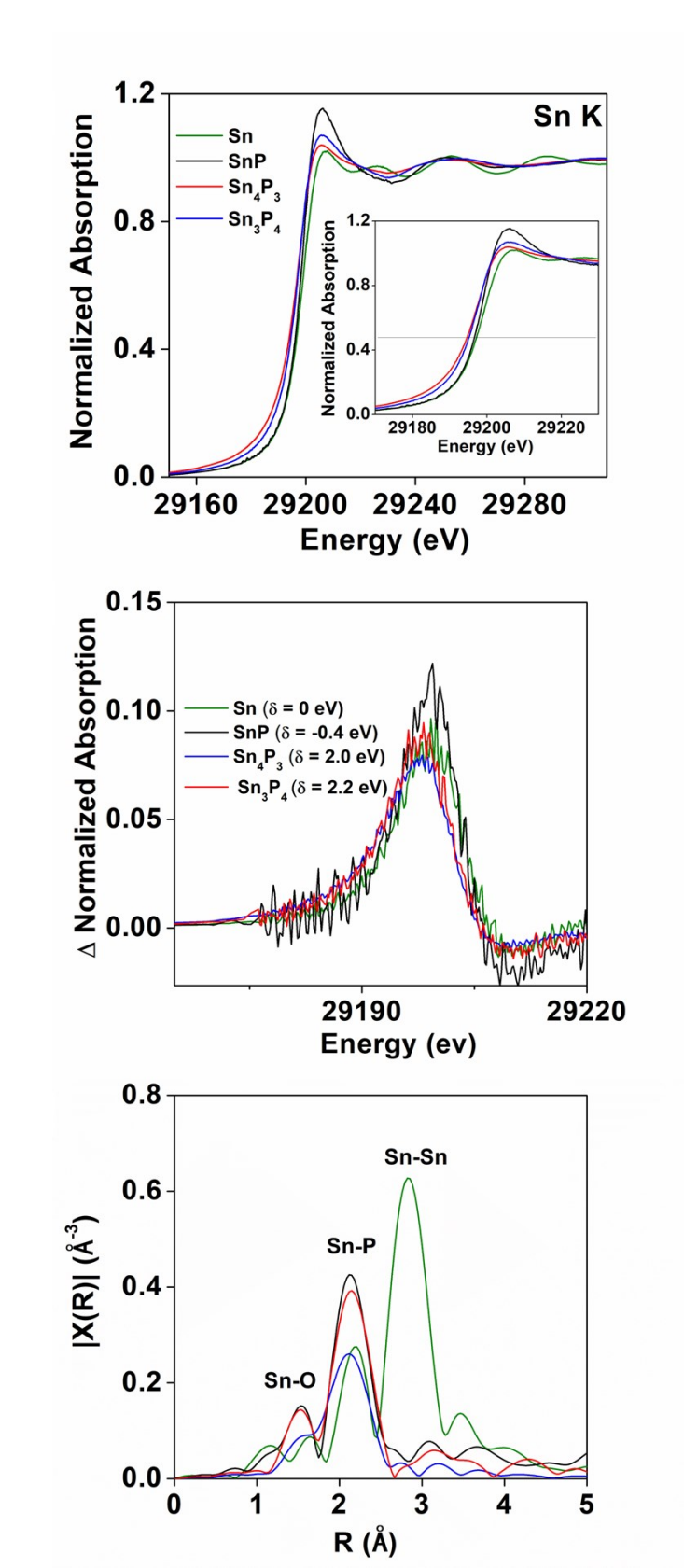


Figure 6. X-ray photoelectron spectroscopy (XPS) spectra observed at the (a) Sn(3d_{5/2}) and (b)

P(2p₃/₂) regions for Sn₃P₄ (bottom, black), SnP (middle, red), Sn₄P₃ (top, blue) nanocrystals. Sn(3d₅/₂) binding energies revealed the presence of mixed oxidation states in all tin phosphides, which displayed binding energies from 484.6 eV to 486.2 eV.

Formal charge(s) of tin in tin phosphides remain under investigation, however Sn²⁺ and Sn⁴⁺ species present in Sn₃P₄ and Sn₃P₄ may have also appeared due to surface oxidation; P(2p₃/₂) binding energies of 133 eV are characteristic of metal phosphates. Still, metal phosphide bonding, characteristic of binding energies below 130 eV, were observed. XAS measurements at the Sn *K*-edge further showed the complexity of the local environment around Sn (Figure 7a). SnP showed metallic behavior as expected; the very small electronegativity difference between tin and phosphorus causes delocalization of the electrons and allows for the layered structure of SnP.⁵⁵ Closer inspection of the X-ray absorption near edge structure (XANES) region in derivative plot further showed this small shift in ionization energy for Sn₄P₃ and Sn₃P₄, unexpectedly to binding energies below that of metallic tin, represented by a reference foil (Figure 7b). Back bonding from

- phosphorus to metals could be a possible explanation for this behavior.⁵⁸ The Sn K-edge XANES
- 2 spectra reflects the transition energy from the 1s state to the 5p state. If back donation occurred, it
- 3 could result in an increased shielding effect that would support our observed red shift. However,
- 4 our XPS data contradict this hypothesis, as back donation implies a positive charge on phosphorus.
- 5 Further investigation is ongoing.
- 6 Despite unusual XANES behavior, the Fourier Transform of the k^2 -weighted Extended X-ray
- 7 absorption fine structure (EXAFS) data (**Figure 7c**) were consistent with Sn-P bonding expected
- 8 for tin phosphides. The position of the first shell peaks at approximately 2.1 Å for Sn₄P₃, SnP, and
- 9 Sn₃P₄ were attributed to the Sn-P photoelectron path. Note that peak positions in **Figure 7c** and
- the actual bond lengths differ by ca. 0.5 Å because of the photoelectron phase shift. The actual
- observed bond lengths for our materials were therefore approximately 2.6 Å, consisted with
- 12 reported Sn-P bond lengths.⁵ A small feature around 1.4 Å that was observed in SnP and Sn₃P₄
- was attributed to the Sn-O photoelectron path.



1 Figure 7. (a) X-ray absorption near edge structure (XANES) spectra taken at the Sn K- edge for 2 Sn₃P₄ (red), Sn₄P₃ (blue), and SnP (black) nanocrystals. The inset shows the normalized absorption 3 spectrum. Data is plotted against Sn foil (Sn⁰ green). (b) The first derivative of the XANES spectra 4 with relative shifts (δ) from the first derivative point of Sn⁰ and (\mathbf{c}) Fourier transform magnitude k^2 -weighted EXAFS spectra (FT-EXAFS). Two first-shell pathways were identified in tin 5 6 phosphides: Sn—O (1.4 Å) and Sn—P (2.1 Å). Note that peak positions in and the actual bond 7 lengths differ by ca. 0.5 Å because of the photoelectron phase shift. The bond lengths for tin 8 phosphide materials are approximately 2.6 Å, consistent with previous reports. 9

10

11

12

13

14

For SnP and Sn₄P₃, fitting was performed using their bulk structures. For Sn₃P₄, a survey of pathways was explored; though XRD data showed a similar structure to that predicted by Huang et al., some peaks remain unindexed. We thus investigated several models to gain insight to local structure in Sn₃P₄ (Table S1). Aside from Sn-P, the scattering contributions of Sn-O were also included in some cases, as oxidation was observed in TEM measurements.

15

16

17

18

19

20

21

22

23

A summary of the fits can be found in **Figure 8**. For SnP, the trigonal phase provided an R-factor of 0.4% (Table S2, Figure 8a, b). The agreement with the trigonal structure was expected as the XRD data for synthesized SnP was indexed to the same phase. The calculated Sn-P coordination number and bond length, however, were larger than expected; we obtained an Sn-P bond length of 2.69 ± 0.13 Å, and a coordination number N of 2.9 ± 0.7 . The structure model had a total of three Sn-P bonds: two shorter bonds and one longer bond with a 0.52 Å difference (i.e., 1.96 Å and 2.52 Å). The influence of k-weighting on the expected Sn-X coordination numbers, N, was investigated and the results indicate overall consistency within the obtained values for N (**Table S3**).

24

25

26

27

Similarly, for Sn₄P₃ the bulk structure model was rhombohedral, as indexing of the XRD directed (Table S4, Figure 8c, d). Even though the expected bond lengths were consistent with predicted Sn-P bonds; the apparent change in coordination number from N=3 to N=1 could be attributed

1 to the decrease in cluster size, but a full understanding of structure would require modeling of higher-order shells unobserved in our nanoparticles.⁵⁹ We hypothesize that these differences may 2 come from Sn-Sn bonding from interlayers of SnP (excluded in our model) but have been 3 previously observed in EXAFS.³⁴ 4 5 6 For Sn₃P₄, we expected the structure to match most closely that of trigonal Sn₃P₄ provided by Huang et al.³⁸ However, the tetragonal phase of SnP provided the best fit with an R-factor of 0.3% 7 8 (Table S5, Figure 8e, f). While our XRD data was insufficient to provide a weight fraction of SnP 9 present, the data suggest that local structure may be closer to that of SnP. Further investigation of 10 the structure is thus needed. We note that to date, crystalline nanoparticles of Sn₃P₄ have not yet 11 been reported. Even in the bulk, the structure of Sn₃P₄ remains unresolved; several phases have 12 been predicted to exist in literature. 13 While the structure of tin phosphides remains to be solved, our measurements provided insight on 14 15 the effect of crystallite size and explored the distinct differences in the local coordination in the 16

the effect of crystallite size and explored the distinct differences in the local coordination in the synthesized tin phosphides. Further understanding of how particle size influences the local environments of Sn in layered tin phosphides will be critical to provide understanding of how intercalation processes in electrochemical systems using these tin phosphides are affected by particle size.

17

18

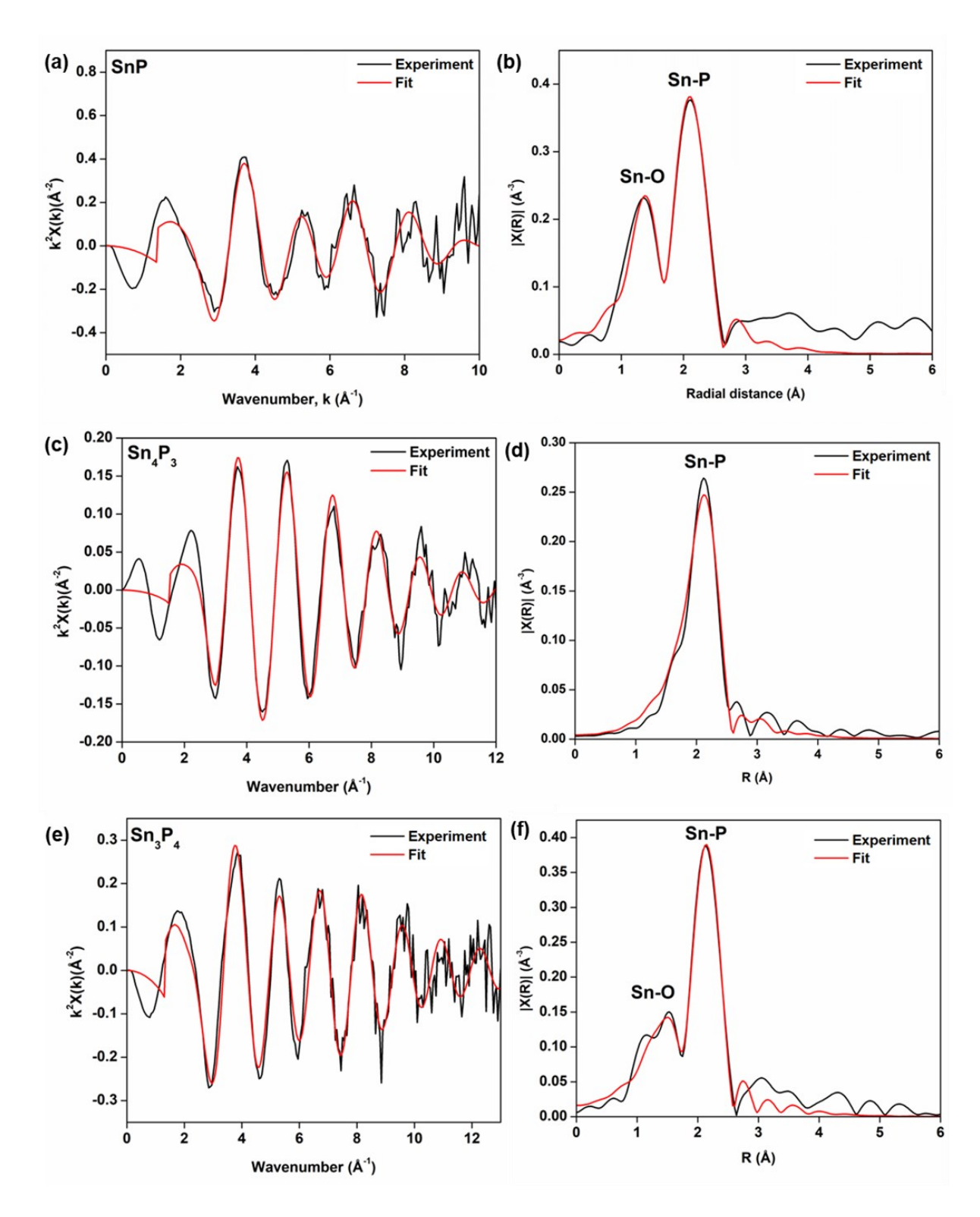


Figure 8. Summary of EXAFS fitting for (**a**, **b**) SnP, (**c**, **d**) Sn₄P₃, and (**e**, **f**) Sn₃P₄ shown in both k and r space. SnP data were fit with an r range of 1.1 to 2.8 Å and k range of 2.0 to 9.0 Å⁻¹. Sn-O and Sn-P photoelectron paths were used in the fit to SnP. Sn₄P₃ data were fit an r range of 1.45 to 3 Å and k range of 2.3 to 11.45 Å⁻¹ Sn-P photoelectron path was used in the fit to Sn₄P₃. Sn₃P₄ fits

- were performed using a k range of 2.5 to 10.5 Å⁻¹ and an r range of 1.1 to 2.7 Å. Sn-O and Sn-P
- 2 photoelectron path were used in the fit for Sn₃P₄.

- 4 Conclusions
- 5 To the best of our knowledge, we report the first use of aminophosphines to achieve significant
- 6 phase flexibility in tin phosphide nanocrystals and obtain Sn₃P₄, SnP, and Sn₄P₃. Understanding
- 7 the mechanisms responsible for each phase requires further investigation. X-ray spectroscopy
- 8 measurements provided insight on the local chemical environments of tin, of interest for further
- 9 study of tin phosphides in applications such as electrochemical reactions.

10 **Author Contributions**

- All authors contributed to the preparation of the manuscript. A. Sahu conceived and supervised
- the project. R. Y. and S. C. performed all preliminary syntheses and characterization. I. J. P., S.
- L., and H. X. optimized syntheses protocols and performed XRD measurements. I. J. P. and S. L.
- performed bright field TEM imaging. I. J. P., A. M. E., and M. K. performed XAS measurements.
- A. I. F. supervised XAS measurements and data analysis. I. J. P. and A. M. P. analyzed XRD data
- 16 for Sn₃P₄, S. H. performed STEM imaging and elemental analysis at BNL. A. Singh performed
- 17 STEM imaging and elemental analysis at LBNL. I. J. P. and A. Sahu analyzed all the data.

18

19

Conflicts of Interest

- 20 The authors declare no competing financial interest.
- 21 Acknowledgements
- 22 I. J. P acknowledges support by the U.S. Department of Energy (DOE), Office of Science, Office
- 23 of Workforce Development for Teachers and Scientists, Office of Science Graduate Student
- Research (SCGSR) program. The SCGSR program is administered by the Oak Ridge Institute for
- 25 Science and Education (ORISE) for the DOE. ORISE is managed by ORAU under contract

number DE-SC0014664. All opinions expressed in this paper are the author's and do not necessarily reflect the policies and views of DOE, ORAU, or ORISE. All the synthetic work by I. J. P and A. Sahu was supported by the National Science Foundation (DMR-2114385). XAS analysis by A. I. F was supported by the National Science Foundation under Grant No. CHE-1903576. This research used beamline 7-BM (QAS) of the National Synchrotron Light Source II, a U.S. DOE Office of Science User Facility operated for the DOE Office of Science by Brookhaven National Laboratory (BNL) under Contract No. DE-SC0012704. The QAS beamline operations were supported in part by the Synchrotron Catalysis Consortium (U.S. DOE, Office of Basic Energy Sciences, grant number DE-SC0012335). The authors acknowledge Steven Ehrlich and Lu Ma of 7-BM for their technical assistance. Work at the Molecular Foundry was supported by the Office of Science, Office of Basic Energy Sciences, of the U.S. Department of Energy under Contract No. DE-AC02-05CH11231. Work by the author H. K. was partially supported by the Schlumberger Foundation Faculty for the Future Program.

We are grateful for the assistance of Tony Hu at the Department of Chemistry of New York University with the X-ray analysis, and we thank the support to the X-ray facility by the National Science Foundation under Award Numbers CRIF/CHE-0840277 and by the NSF MRSEC Program under Award Number DMR-0820341 and DMR-1420073. The authors would also like to acknowledge Tai-De Li, Sheng Zheng, and Tong Wang of the Imaging and Surface Science Facilities of CUNY Advanced Science Research Center for assistance with instrument use and scientific and technical assistance. Lastly, we acknowledge Yuan Ping Feng and Huang Min for sharing the structure files for predicted crystal structures of Sn₃P₄.

1 **Supporting Information**

- 2 Supporting Information (ESI) available Includes detailed information on the experimental
- 3 methods used: X-ray diffraction (XRD), Transmission electron microscopy (TEM), X-ray
- 4 photoelectron spectroscopy (XPS), X-ray absorption spectroscopy (XAS), Scherrer Analysis,
- 5 TEM figures, XRD figures and EXAFS data analysis (Figures and Tables).

References

- 7 1. Zhao, X.; Yang, Q.; Quan, Z., Tin-based nanomaterials: colloidal synthesis and battery applications. *Chemical Communications* **2019**, *55* (60), 8683-8694.
- 9 2. Huang, B.; Pan, Z.; Su, X.; An, L., Tin-based materials as versatile anodes for alkali (earth)-ion batteries. *Journal of Power Sources* **2018**, *395*, 41-59.
- 3. Zaikina, J. V.; Kovnir, K. A.; Sobolev, A. N.; Presniakov, I. A.; Kytin, V. G.; Kulbachinskii,
- 12 V. A.; Olenev, A. V.; Lebedev, O. I.; Tendeloo, G. V.; Dikarev, E. V.; Shevelkov, A. V.,
- Highly Disordered Crystal Structure and Thermoelectric Properties of Sn₃P₄. *Chemistry of Materials* **2008**, *20* (7), 2476-2483.
- 15 4. Bougherara, K.; Rai, D. P.; Reshak, A. H., First principles prediction of the elastic, electronic
- and optical properties of Sn_3X_4 (X = P, As, Sb, Bi) compounds: Potential photovoltaic absorbers. *Chinese Journal of Physics* **2019**, *59*, 265-272.
- 18 5. Kamitani, M.; Bahramy, M. S.; Nakajima, T.; Terakura, C.; Hashizume, D.; Arima, T.;
- Tokura, Y., Superconductivity at the Polar-Nonpolar Phase Boundary of SnP with an Unusual Valence State. *Physical Review Letters* **2017**, *119* (20), 207001.
- 6. Liu, S.; Li, S.; Li, M.; Yan, L.; Li, H., Synthesis of tin phosphides (Sn4P3) and their high photocatalytic activities. *New Journal of Chemistry* **2013**, *37* (3), 827-833.
- 7. Zhang, R.; Yu, G.; Gao, Y.; Huang, X.; Chen, W., Applying surface strain and coupling with
- pure or N/B-doped graphene to successfully achieve high HER catalytic activity in 2D layered
- SnP₃-based nanomaterials: a first-principles investigation. *Inorganic Chemistry Frontiers* **2020**.
- 8. Liu, J.; Yu, G.; Zhang, R.; Huang, X.; Chen, W., Theoretical predication of the high hydrogen
- evolution catalytic activity for the cubic and tetragonal SnP systems. *Physical Chemistry Chemical Physics* **2019**, *21* (10), 5521-5530.
- 9. Ye, Z.; Jiang, Y.; Feng, T.; Wang, Z.; Li, L.; Wu, F.; Chen, R., Curbing polysulfide shuttling
- by synergistic engineering layer composed of supported Sn₄P₃ nanodots electrocatalyst in lithium-sulfur batteries. *Nano Energy* **2020**, *70*, 104532.
- 33 10. Ran, L.; Luo, B.; Gentle, I. R.; Lin, T.; Sun, Q.; Li, M.; Rana, M. M.; Wang, L.; Knibbe,
- R., Biomimetic Sn₄P₃ Anchored on Carbon Nanotubes as an Anode for High-Performance
- 35 Sodium-Ion Batteries. ACS Nano **2020**, 14 (7), 8826-8837.
- 36 11. Zhou, W. C.; Yang, H. X.; Shao, S. Y.; Ai, X. P.; Cao, Y. L., Superior high rate capability
- of tin phosphide used as high capacity anode for aqueous primary batteries. *Electrochemistry Communications* **2006**, *8* (1), 55-59.
- 39 12. Ueda, A.; Nagao, M.; Inoue, A.; Hayashi, A.; Seino, Y.; Ota, T.; Tatsumisago, M.,
- Electrochemical performance of all-solid-state lithium batteries with Sn₄P₃ negative electrode.
- 41 *Journal of Power Sources* **2013,** *244*, 597-600.

- 1 13. Kim, Y.; Kim, Y.; Choi, A.; Woo, S.; Mok, D.; Choi, N.-S.; Jung, Y. S.; Ryu, J. H.; Oh, S. M.; Lee, K. T., Tin Phosphide as a Promising Anode Material for Na-Ion Batteries.

 Advanced Materials 2014, 26 (24), 4139-4144.
- 4 14. Qian, J.; Xiong, Y.; Cao, Y.; Ai, X.; Yang, H., Synergistic Na-Storage Reactions in Sn₄P₃ as a High-Capacity, Cycle-stable Anode of Na-Ion Batteries. *Nano Letters* **2014**, *14* (4), 1865-1869.
- 15. Fan, X.; Gao, T.; Luo, C.; Wang, F.; Hu, J.; Wang, C., Superior reversible tin phosphide-carbon spheres for sodium ion battery anode. *Nano Energy* **2017**, *38*, 350-357.
- 9 16. Fan, X.; Mao, J.; Zhu, Y.; Luo, C.; Suo, L.; Gao, T.; Han, F.; Liou, S.-C.; Wang, C., Superior Stable Self-Healing SnP₃ Anode for Sodium-Ion Batteries. *Advanced Energy Materials* **2015**, *5* (18), 1500174.
- 17. Li, B.; Shang, S.; Zhao, J.; Itkis, D. M.; Jiao, X.; Zhang, C.; Liu, Z.-K.; Song, J., Metastable trigonal SnP: A promising anode material for potassium-ion battery. *Carbon* **2020**.
- 18. Lan, D.; Wang, W.; Shi, L.; Huang, Y.; Hu, L.; Li, Q., Phase pure Sn₄P₃ nanotops by solution-liquid-solid growth for anode application in sodium ion batteries. *Journal of Materials Chemistry A* **2017**, *5* (12), 5791-5796.
- 19. Liu, S.; Zhang, H.; Xu, L.; Ma, L.; Hou, X., High Lithium Storage Performance of Mn-doped Sn₄P₃ nanoparticles. *Electrochimica Acta* **2016**, *210* (Supplement C), 888-896.
- 20. Liu, S.; Zhang, H.; Xu, L.; Ma, L., Synthesis of hollow spherical tin phosphides (Sn₄P₃) and their high adsorptive and electrochemical performance. *Journal of Crystal Growth* **2016**, *438* (Supplement C), 31-37.
- 21. Liu, S.; Zhang, H.; Xu, L.; Ma, L.; Chen, X., Solvothermal preparation of tin phosphide as a long-life anode for advanced lithium and sodium ion batteries. *Journal of Power Sources* **2016**, 304, 346-353.
- 22. Xu, Y.; Peng, B.; Mulder, F. M., A High-Rate and Ultrastable Sodium Ion Anode Based on a Novel Sn₄P₃-P@Graphene Nanocomposite. *Advanced Energy Materials* **2018**, *8* (3), 1701847.
- 23. Ding, Y.; Li, Z.-F.; Timofeeva, E. V.; Segre, C. U., In Situ EXAFS-Derived Mechanism of
 Highly Reversible Tin Phosphide/Graphite Composite Anode for Li-Ion Batteries. *Advanced Energy Materials* 2018, 8.
- 24. Pan, E.; Jin, Y.; Zhao, C.; Jia, M.; Chang, Q.; Zhang, R.; Jia, M., Mesoporous Sn₄P₃ graphene aerogel composite as a high-performance anode in sodium ion batteries. *Applied Surface Science* 2019, 475, 12-19.
- 25. Chojnacka, A.; Pan, X.; Jeżowski, P.; Béguin, F., High performance hybrid sodium-ion capacitor with tin phosphide used as battery-type negative electrode. *Energy Storage Materials* **2019**, *22*, 200-206.
- 26. Jiang, Y.; Wang, Y.; Jiang, J.; Liu, S.; Li, W.; Huang, S.; Chen, Z.; Zhao, B., In-situ solvothermal phosphorization from nano-sized tetragonal-Sn to rhombohedral-Sn₄P₃ embedded in hollow graphene sphere with high capacity and stability. *Electrochimica Acta* **2019**, *312*, 263-271.
- 27. Usui, H.; Domi, Y.; Yamagami, R.; Sakaguchi, H., Degradation mechanism of tin phosphide as Na-ion battery negative electrode. *Green Energy & Environment* **2019**.
- 28. Usui, H.; Domi, Y.; Fujiwara, K.; Shimizu, M.; Yamamoto, T.; Nohira, T.; Hagiwara, R.; Sakaguchi, H., Charge–Discharge Properties of a Sn₄P₃ Negative Electrode in Ionic Liquid
- Electrolyte for Na-Ion Batteries. ACS Energy Letters 2017, 2 (5), 1139-1143.

- 29. Saddique, J.; Zhang, X.; Wu, T.; Su, H.; Liu, S.; Zhang, D.; Zhang, Y.; Yu, H., Sn₄P₃induced crystalline/amorphous composite structures for enhanced sodium-ion battery anodes. *Journal of Materials Science & Technology* **2019**.
- 30. Yadav, P.; Malik, W.; Dwivedi, P. K.; Jones, L. A.; Shelke, M. V., Electrospun Nanofibers of Tin Phosphide (SnP_{0.94}) Nanoparticles Encapsulated in a Carbon Matrix: A Tunable Conversion-cum-Alloying Lithium Storage Anode. *Energy & Fuels* **2020**, *34* (6), 7648-7657.
- 7 31. Zhao, X.; Wang, W.; Hou, Z.; Wei, G.; Yu, Y.; Zhang, J.; Quan, Z., SnP_{0.94} 8 nanoplates/graphene oxide composite for novel potassium-ion battery anode. *Chemical Engineering Journal* **2019**, *370*, 677-683.
- 32. Zhang, M.; Wang, H.; Feng, J.; Chai, Y.; Luo, X.; Yuan, R.; Yang, X., Controllable synthesis of 3D nitrogen-doped carbon networks supported Sn_xP_y nanoparticles as high performance anode for lithium ion batteries. *Applied Surface Science* **2019**, *484*, 899-905.
- 33. Aso, K.; Kitaura, H.; Hayashi, A.; Tatsumisago, M., SnP_{0.94} active material synthesized in high-boiling solvents for all-solid-state lithium batteries. **2010**, 118, 620-622.
- 34. Kim, Y.; Hwang, H.; Yoon, C. S.; Kim, M. G.; Cho, J., Reversible Lithium Intercalation in
 Teardrop-Shaped Ultrafine SnP_{0.94} Particles: An Anode Material for Lithium-Ion Batteries.
 Advanced Materials 2007, 19 (1), 92-96.
- 35. Shin, H.-S.; Jung, K.-N.; Jo, Y. N.; Park, M.-S.; Kim, H.; Lee, J.-W., Tin phosphide-based anodes for sodium-ion batteries: synthesis via solvothermal transformation of Sn metal and phase-dependent Na storage performance. **2016**, *6*, 26195.
- 36. Liang, J.-M.; Zhang, L.-J.; XiLi, D.-G.; Kang, J., Research progress on tin-based anode materials for sodium ion batteries. *Rare Metals* **2020**, *39* (9), 1005-1018.
- 23 37. Yang, R.; Ma, Y.; Wei, Q.; Zhang, D., A first-principles investigation of the properties of two predicted novel structures of Sn3P4. *Chinese Journal of Physics* **2018**, *56* (3), 886-894.
- 38. Huang, M.; Feng, Y. P., Stability and electronic properties of Sn3P4. *Physical Review B* 2004,
 70 (18), 184116.
- 39. Tallapally, V.; Esteves, R. J. A.; Nahar, L.; Arachchige, I. U., Multivariate Synthesis of Tin Phosphide Nanoparticles: Temperature, Time, and Ligand Control of Size, Shape, and Crystal Structure. *Chemistry of Materials* **2016**, *28* (15), 5406-5414.
- 40. Liu, J.; Wang, S.; Kravchyk, K.; Ibáñez, M.; Krumeich, F.; Widmer, R.; Nasiou, D.; Meyns,
 M.; Llorca, J.; Arbiol, J.; Kovalenko, M. V.; Cabot, A., SnP nanocrystals as anode materials
 for Na-ion batteries. *Journal of Materials Chemistry A* 2018, 6 (23), 10958-10966.
- 41. Su, H. L.; Xie, Y.; Li, B.; Liu, X. M.; Qian, Y. T., A Novel One-Step Solvothermal Route to
 Nanocrystalline Sn4P3. *Journal of Solid State Chemistry* 1999, 146 (1), 110-113.
- 42. Song, W.-S.; Lee, H.-S.; Lee, J. C.; Jang, D. S.; Choi, Y.; Choi, M.; Yang, H., Amine-derived synthetic approach to color-tunable InP/ZnS quantum dots with high fluorescent qualities. *Journal of Nanoparticle Research* **2013**, *15* (6), 1750.
- 43. Tessier, M. D.; De Nolf, K.; Dupont, D.; Sinnaeve, D.; De Roo, J.; Hens, Z., Aminophosphines: A Double Role in the Synthesis of Colloidal Indium Phosphide Quantum Dots. *Journal of the American Chemical Society* **2016**, *138* (18), 5923-5929.
- 44. Buffard, A.; Dreyfuss, S.; Nadal, B.; Heuclin, H.; Xu, X.; Patriarche, G.; Mézailles, N.; Dubertret, B., Mechanistic Insight and Optimization of InP Nanocrystals Synthesized with Aminophosphines. *Chemistry of Materials* **2016**, *28* (16), 5925-5934.
- 45. Tessier, M. D.; Dupont, D.; De Nolf, K.; De Roo, J.; Hens, Z., Economic and Size-Tunable Synthesis of InP/ZnE (E = S, Se) Colloidal Quantum Dots. *Chemistry of Materials* **2015**, *27* (13), 4893-4898.

- 46. Mundy, M. E.; Ung, D.; Lai, N. L.; Jahrman, E. P.; Seidler, G. T.; Cossairt, B. M., Aminophosphines as Versatile Precursors for the Synthesis of Metal Phosphide Nanocrystals. *Chemistry of Materials* **2018**, *30* (15), 5373-5379.
- 4 47. Rachkov, A. G.; Schimpf, A. M., Colloidal Synthesis of Tunable Copper Phosphide Nanocrystals. *Chemistry of Materials* **2021**.
- 48. Park, Y.; Kang, H.; Hong, Y.-k.; Cho, G.; Choi, M.; Cho, J.; Ha, D.-H., Influence of the phosphorus source on iron phosphide nanoparticle synthesis for hydrogen evolution reaction catalysis. *International Journal of Hydrogen Energy* **2020**.
- 9 49. Laufersky, G.; Bradley, S.; Frécaut, E.; Lein, M.; Nann, T., Unraveling aminophosphine 10 redox mechanisms for glovebox-free InP quantum dot syntheses. *Nanoscale* **2018**, *10* (18), 11 8752-8762.
- 50. Donohue, P. C., Synthesis, structure, and superconducting properties of new high-pressure forms of tin phosphide. *Inorganic Chemistry* **1970**, *9* (2), 335-337.
- S1. Reiss, P.; Carrière, M.; Lincheneau, C.; Vaure, L.; Tamang, S., Synthesis of Semiconductor
 Nanocrystals, Focusing on Nontoxic and Earth-Abundant Materials. *Chemical Reviews* 2016,
 116 (18), 10731-10819.
- 52. Ritscher, A.; Schmetterer, C.; Ipser, H., Pressure dependence of the tin–phosphorus phase diagram. *Monatshefte für Chemie Chemical Monthly* **2012**, *143* (12), 1593-1602.
- 53. Thanh, T. K. Nguyen; Maclean, N.; Mahiddine, S. Mechanisms of Nucleation and Growth of Nanoparticles in Solution. *Chemical Reviews* **2014**, 114, 7610-7630.
- 54. R. I. Hegde, Core Level Binding Energy Shifts in Dilute Tin Alloys, Surface and Interface
 Analysis 1982, 4, 205 207.
- 55. Häggström, L.; Gullman, J.; Ericsson, T.; Wäppling, R., Mössbauer study of tin phosphides.
 Journal of Solid State Chemistry 1975, *13* (3), 204-207.
- 56. Kim, Y.-U.; Lee, C. K.; Sohn, H.-J.; Kang, T., Reaction Mechanism of Tin Phosphide Anode by Mechanochemical Method for Lithium Secondary Batteries. *Journal of The Electrochemical Society* **2004**, *151* (6), A933-A937.
- 57. Ma, L.; Yan, P.; Wu, S.; Zhu, G.; Shen, Y., Engineering tin phosphides@carbon yolk—shell nanocube structures as a highly stable anode material for sodium-ion batteries. *Journal of Materials Chemistry A* **2017**, *5* (32), 16994-17000.
- 58. Blanchard, P. E. R.; Grosvenor, A. P.; Cavell, R. G.; Mar, A., X-ray Photoelectron and Absorption Spectroscopy of Metal-Rich Phosphides M2P and M3P (M = Cr–Ni). *Chemistry of Materials* **2008**, *20* (22), 7081-7088.
- 59. Frenkel, A.; Yevick, A.; Cooper, C.; Vasic, R. Modeling the Structure and Composition of Nanoparticles by Extended Absorption Fine-Structure Spectroscopy. *Annual Reviews* **2011**, *4*, 23-29.